

DOI: 10.13208/j.electrochem.151245

Cite this: *J. Electrochem.* **2016**, 22(3): 278-287

Artical ID:1006-3471(2016)03-0278-10

Http://electrochem.xmu.edu.cn

## Reduced Graphene Oxide (RGO) Hollow Network Cages for High-Performance Electrochemical Energy Storage

Chi Zhang, Xu-Jun He, Gao-Ren Li\*

(School of Chemistry and Chemical Engineering, Sun Yat-sen University, Guangzhou 510275, China)

**Abstract:** The reduced graphese oxide (RGO) hollow network cages were synthesized via zinc oxide (ZnO) template-assisted electrodeposition. The as-prepared RGO hollow network cages exhibited the multi-level architectures, from nano sheets, porous structures, networks, to 3D microscaled hollow cages, which can simultaneously optimize transport of electroactive species, utilization rate of electrode material, and super capacitive performance. Electrochemical measurements confirmed the superior performance of RGO hollow network cages for supercapacitors (SCs), such as high  $C_{sp}$  ( $393 \text{ F} \cdot \text{g}^{-1}$  at  $1.0 \text{ A} \cdot \text{g}^{-1}$ ), excellent rate capability ( $21.2\% C_{sp}$  loss from  $1.0$  to  $20 \text{ A} \cdot \text{g}^{-1}$ ), and superior cycling stability ( $< 1\% C_{sp}$  loss after 10000 cycles).

**Key words:** reduced graphene oxide; porous structure; nanotube; supercapacitor

**CLC Number:** Q81; O646.54

**Document Code:** A

Graphene, a two-dimensional (2D) monolayer form of  $\text{sp}^2$ -hybridized carbon atoms, has fascinating mechanical and electronic properties because of its unique structure and is, therefore, highly promising for various applications, such as energy storage/conversion, electronics, and ultrasensitives sensors<sup>[1-5]</sup>. Graphene as an electrode material is a good candidate for supercapacitors (SCs) because of its high theoretical specific capacitance ( $C_{sp}$ ) of about  $526 \text{ F} \cdot \text{g}^{-1}$ . However, the reported graphene materials could only attain 20% to 60% of the theoretical value, especially when they were prepared in the form of reduced graphene oxide (RGO)<sup>[6-11]</sup>. During the fabrication of electrodes, graphene sheets are easily to form agglomerates or to restack to form graphite through the van der Waals interactions. In such cases, it would be difficult for ions to gain access to inner layers. This not only leads to a negative influence on  $C_{sp}$ , but also causes a loss in rate capability of SCs<sup>[12-18]</sup>. Recently, some researchers have tried to prevent graphene from restacking by introducing carbon nanotubes (CNTs)<sup>[19-21]</sup>. However, the utilized fabrication techniques usually

require multiple steps and most of the fabricated CNTs/graphene composites represent a separated morphologies for CNTs and graphene, leading to the loss of surface area because of graphene and CNTs aggregations.

The integration of graphene sheets into functional nanostructures is an efficient approach to avoid the agglomeration of graphene, and it has attracted a tremendous amount of attention from researchers<sup>[22-28]</sup>. On the road to electrochemical energy storage, the hollow nanostructures appear to hold the edge over other forms in terms of performance, and they can considerably favour the diffusion of electroactive species into the inner of electrode and the accessibility to much more active sites<sup>[29-33]</sup>. The hollow nanostructures also can largely enhance external surface areas, increase active sites, and significantly reduce diffusion path length<sup>[34-38]</sup>. Therefore, the graphene hollow nanostructures as electrodes will be highly attractive for SCs. However, up to now, it still remains a great challenge to find a facile method to fabricate the well defined hollow nanostructures of graphene

Received: 2016-01-12, Revised: 2016-05-30 \*Corresponding author, tel: , E-mail: ligaoren@mail.sysu.edu.cn

This work was supported by National Natural Science Foundation of China (No. 51173212), National Basic Research Program of China (No. 2015CB932304), Natural Science Foundation of Guangdong Province (Nos. S2013020012833 and 2016A010104004), and Fundamental Research Fund for the Central Universities (No. 16lgjc67)

or RGO.

Inspired by the above consideration, here we firstly report the synthesis of RGO hollow network cages on conductive substrate via ZnO template assisted electrochemical reduction of graphene oxide (GO). The fabricated RGO hollow network cages were a kind of novel hollow nanostructures and they possessed multilevel architectures, from nanosheets, porous structures, networks, to 3D micro-scaled hollow cages, which will simultaneously optimize transport of electroactive species, utilization rate of electrode material, and supercapacitive properties. Importantly, the template assisted electrochemical reduction method for the fabrication of such RGO hollow network cages is facile, low-cost, green and scalable, providing a new opportunity for the rational design and engineering of graphene materials with enhanced performance. The results in this paper demonstrate that the RGO hollow network cages exhibited superior supercapacitive performance and long-term cycle stability because of the special geometrical properties (i.e. networks and hollow cage structures). To the best of our knowledge, this is the first report on the synthesis of RGO hollow network cages for SCs.

## 1 Experimental

### 1.1 Synthesis of Hollow Graphene Network Cages (HGNCs)

All chemical reagents were of analytical (AR) grade. Electrochemical deposition was carried out in a simple two-electrode electrolytic cell via galvanostatic electrodeposition, and the graphite electrode was used as a counter electrode (spectral grade, 1.8 cm<sup>2</sup>). The porous HGNCs were fabricated by the procedures described as follows:

The ZnO nanorod arrays (NRAs) template was electrodeposited in solutions of 0.01 mol · L<sup>-1</sup> Zn(NO<sub>3</sub>)<sub>2</sub> + 0.05 mol · L<sup>-1</sup> NH<sub>4</sub>NO<sub>3</sub> with current density of 0.5 mA · cm<sup>-2</sup> at 70 °C for 90 min. The Ti plates (99.99%, 1.5 cm<sup>2</sup>) were used as the substrates for electrodeposition, and they were prepared complying the following steps before each experiment: firstly polished by SiC abrasive papers from 300 to 800 grits, then dipped in HCl solution (5%) for 10 min and rinsed

with acetone in ultrasonic bath for 5 min, and finally washed by distilled water.

The ZnO@graphene core-shell NRAs were fabricated by electrodeposition of graphene on the surfaces of ZnO nanorods in solutions of 0.1 g · L<sup>-1</sup> graphene oxide + 0.5 mol · L<sup>-1</sup> Na<sub>2</sub>SO<sub>4</sub> at current density of 2.0 mA · cm<sup>-2</sup> at 298 K for 10 min. The fabricated ZnO@graphene NRAs were immersed in 2.5% aqueous ammonia for 30 min to completely remove ZnO NRAs, and finally the HGNCs were fabricated.

### 1.2 Structural Characterization

The surface morphologies and microstructures of the fabricated HGNCs were characterized by field emission scanning electron microscope (FE-SEM, JSM-6330F) and transmission electron microscope (TEM, JEM-2010HR), respectively. The fabricated nanomaterials were also characterized by Fourier transform infrared spectrometer (FT-IR, Nicolet 330), Raman spectrometer (Renishawin Via), and X-ray diffraction spectrometer (XRD, PIGAKU, D/MAX 2200 VPC).

### 1.3 Electrochemical Characterization

The electrochemical properties of the HGNCs were studied by a CHI 760D electrochemical workstation by cyclic voltammetry in a standard three-electrode cell at room temperature. A graphite sheet was used as the counter electrode and a saturated calomel electrode (SCE) was used as the reference electrode. The HGNCs were used as the working electrode, and the loading was 0.05 mg. The cyclic voltammetric experiments were performed in 0.5 mol · L<sup>-1</sup> Na<sub>2</sub>SO<sub>4</sub> at a scan rate of 5 ~ 100 mV · s<sup>-1</sup>. The average specific capacitance ( $C_{sp}$ ) determined from the cyclic voltammetric curves are calculated according to Eq. (1):

$$C_{sp} = \frac{1}{w\Delta V} \int_y^x i dt \quad (1)$$

where  $i$ ,  $\Delta V$ , and  $w$  are the current (mA), the voltage range of one scanning segment (V), and weight of the electrode material (mg), respectively. The  $C_{sp}$ , energy density ( $d_e$ ), and power density ( $d_p$ ) are also calculated from the chronopotentiometric curves according to Eqs (2 ~ 4):

$$C_{sp} = \frac{I\Delta t}{w\Delta V} \quad (2)$$

$$d_c = \frac{1}{2}C_{sp}(\Delta V)^2 \quad (3)$$

$$d_p = \frac{de}{\Delta t} \quad (4)$$

where  $I$  is the charge/discharge current (mA),  $\Delta t$  is the time for a full charge or discharge (s),  $w$  is the mass of the active electrode material (mg), and  $\Delta V$  is the voltage change after a full charge or discharge (V).

## 2 Results and Discussion

The experimental procedure for the synthesis of RGO hollow network cages is shown in Fig. 1A. The details of fabrication were described in the experimental section in supporting information. The ZnO microrod arrays (MRAs) were firstly fabricated on a conductive substrate as shown in Fig. 1B and they were utilized as templates. Then the electrodeposition of RGO was carried out on the surfaces of ZnO MRAs to form ZnO/RGO composite MRAs. Electrodeposition of RGO on ZnO MRAs was studied by cyclic voltammetry (CV) in the solution of  $0.1 \text{ g} \cdot \text{L}^{-1} \text{ GO} + 0.5 \text{ mol} \cdot \text{L}^{-1} \text{ Na}_2\text{SO}_4$  with the potentials scanning from  $-1.0$  to  $0.2 \text{ V}$  vs SCE at  $100 \text{ mV} \cdot \text{s}^{-1}$ , and the result is shown in Fig. S1. A reduction peak appeared at  $-0.37 \text{ V}$ , and corresponded to the formation of graphene via GO electroreduction, indicating that the RGO can be fabricated on the ZnO template by electrochemical reduction. SEM images of the fabricated ZnO/RGO composites with different deposition time are shown in Fig. S2-4. When the deposition time was 30 s, the RGO thin layers were coated on the surfaces of ZnO MRAs as shown in Fig. S2. With the deposition time increasing, the RGO layers became thicker and thicker. When the deposition time was 10 min, the ZnO MRAs had uniform RGO wraps with porous structures as shown in Fig. 1C. The RGO wraps favorably shared the surfaces of ZnO microrods, and few RGO was packed in the interspaces of microrods, which suggests that the RGO is preferentially deposited on the surfaces of ZnO microrods. Here, the fabricated RGO was self-assembled to form 3D networks on the surfaces of ZnO MRAs. Finally, the RGO hollow network cages were successfully

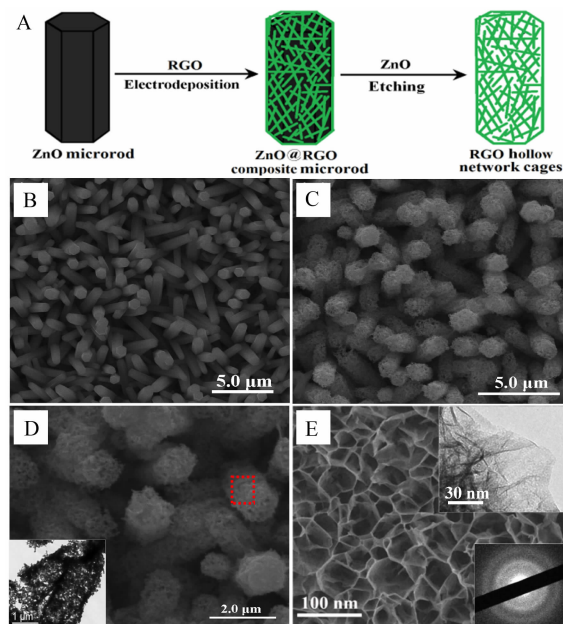


Fig. 1 A. Illustration a synthesis route for the formation of RGO hollow network cages; B. SEM image of the ZnO template; C. SEM image of the ZnO/RGO composite MRAs; D. SEM and TEM (inset) images of the RGO hollow network cages; E. SEM image with a high magnification showing the surface of RGO hollow network cages (The top inset is the TEM image of RGO nanosheet, and the bottom inset is the SAED of RGO nanosheet)

fabricated by dissolving ZnO from ZnO/RGO composite MRAs in 2.5% aqueous ammonia.

Typical SEM and TEM images of the RGO hollow network cages are shown in Fig. 1D, which clearly shows the porous and hollow structures. The lengths of RGO hollow network cages are  $\sim 3.0 \mu\text{m}$  and the diameters are  $\sim 1.0 \mu\text{m}$ . The magnified SEM image showing the surface of RGO hollow network cages is presented in Fig. 1E, which shows nanosheet network structures. The RGO nanosheets were also confirmed by the TEM image shown in top inset in Fig. 1E. Selected area electron diffraction (SAED) image is shown in the bottom inset in Fig. 1E and it indicates the polycrystalline structure of RGO nanosheet. Nitrogen adsorption-desorption isotherm of the RGO hollow network cages is shown in Fig. 2A. The Brunauer-Emmett-Teller (BET) analysis reveals a high specific surface area of  $382 \text{ m}^2 \cdot \text{g}^{-1}$ . The pore size distribution in the inset in Fig. 2A indicates

that the maximal peak appeared at 10 nm. The high specific surface area and appropriate small pore size of RGO hollow network cages will allow high utilization rate of electrode material and rapid diffusion of ions across electrode. In addition, the network structures will be effective in enhancing electron transfer. These features are crucial to improve the performance of SCs as discussed below.

Fig. 2B compares XRD pattern of the RGO hollow network cages (1) with that of GO films (2). The complete disappearance of the characteristic (002) peak at  $2\theta = 10.5^\circ$  suggests the successful conversion of GO to graphene after electroreduction. Also, the graphene (002) broad peak appeared at  $25.2^\circ$  ( $2\theta$ ), which indicates the conversion of GO to graphene. The IR spectra of RGO hollow network cages and GO films are presented in Fig. 2C. As we all know, GO composes of various oxygen containing functional groups, such as ether, epoxide, carboxylic acid, phenolate and aldehyde groups. The IR spectrum of GO films indicates the existence of C-H, C=C, C=O

and C-O groups. However, after electroreduction, the signals related to the C-H, C=O and C-O groups almost disappeared in the RGO hollow network cages, while the signal to the C-C group was clearly seen. Therefore, the above results also demonstrate that the RGO hollow network cages were successfully fabricated. Raman spectra of RGO hollow network cages and GO films are shown in Fig. 2D, which shows the characteristic D and G bands for the RGO hollow network cages and GO films. The intensity ratio of D band to G band usually reflects the order of defects in GO or graphene<sup>[42]</sup>. The calculated value in the intensity ratio of D to G peaks ( $I_D/I_G$ ) for GO is 1.01, while that for the RGO hollow network cages only 0.62, indicating a decrease in the defect level and an increase in the number of graphene layers in the RGO hollow network cages. In addition, the G band of RGO hollow network cages shifted by  $\sim 7\text{ cm}^{-1}$  compared with that of GO films. The blue-shift of G band can be attributed to the conversion of graphite to graphene sheets or the resonance of isolated double bonds at

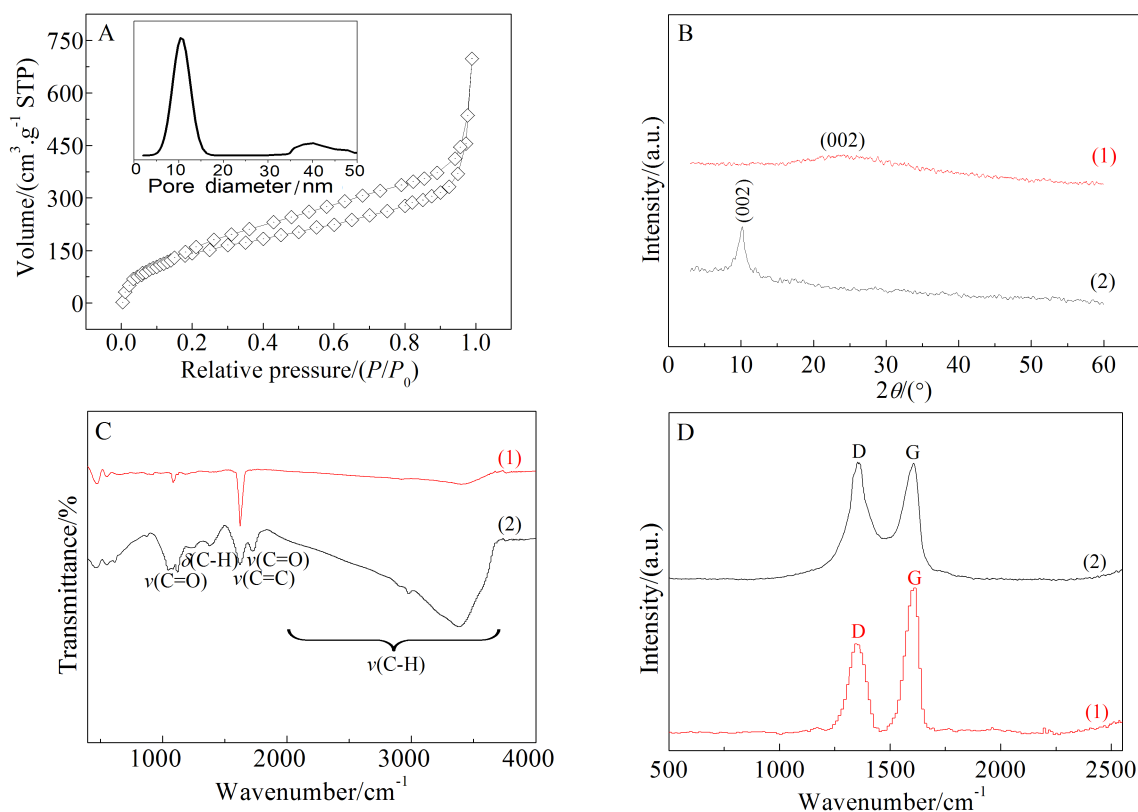


Fig. 2 A. Nitrogen adsorption-desorption isotherm of RGO hollow network cages and pore size distribution (the inset); B. XRD patterns; C-D. IR spectra and Raman spectra of RGO hollow network cages (1) and GO films (2)

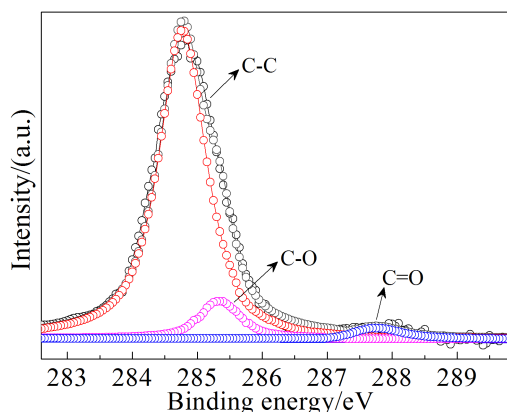


Fig. 3 Fitted XPS spectra of C1s for the RGO hollow network cages

higher frequencies<sup>[42]</sup>. Therefore, both the changes in Raman band intensity and the blue shift of G band provide clear evidence for the presence of graphene in the RGO hollow network cages.

The XPS spectrum of the RGO hollow network cages in C 1s region was measured and is fitted as shown in Fig. 3. The symmetric C 1s peak at 284.64 eV is clearly seen for C—C bond, demonstrating the

existence of graphene in the RGO. Additionally, the oxygen functionalities attached to the carbons show small deconvoluted peaks for C—O (285.3 eV) and C=O (289.7 eV) at higher binding energies, indicating the existence of small amounts of oxygenated carbon species in the RGO. The atomic ratio of C/O represents the reduction degree of GO. On the basis of previous reports, the C/O ratio for hydrazine-reduced GO was about 3.62<sup>[42]</sup>, while, here, the C/O ratio of the RGO hollow network cages was 15.84. Therefore, these fabricated RGO hollow network cages exhibited very high degree of reduction.

The material with high specific surface area, hollow structures, porous structures and three-dimensional networks should be an ideal electrode for SCs. CVs of the RGO hollow network cages and RGO films obtained in 0.5 mol · L<sup>-1</sup> Na<sub>2</sub>SO<sub>4</sub> electrolyte at 5 mV · s<sup>-1</sup> are shown in Fig. 4A, which shows the nearly rectangular shape, indicating the symmetric current-potential characteristics and good capacitive properties. The specific capacitance ( $C_{sp}$ ) of RGO hollow

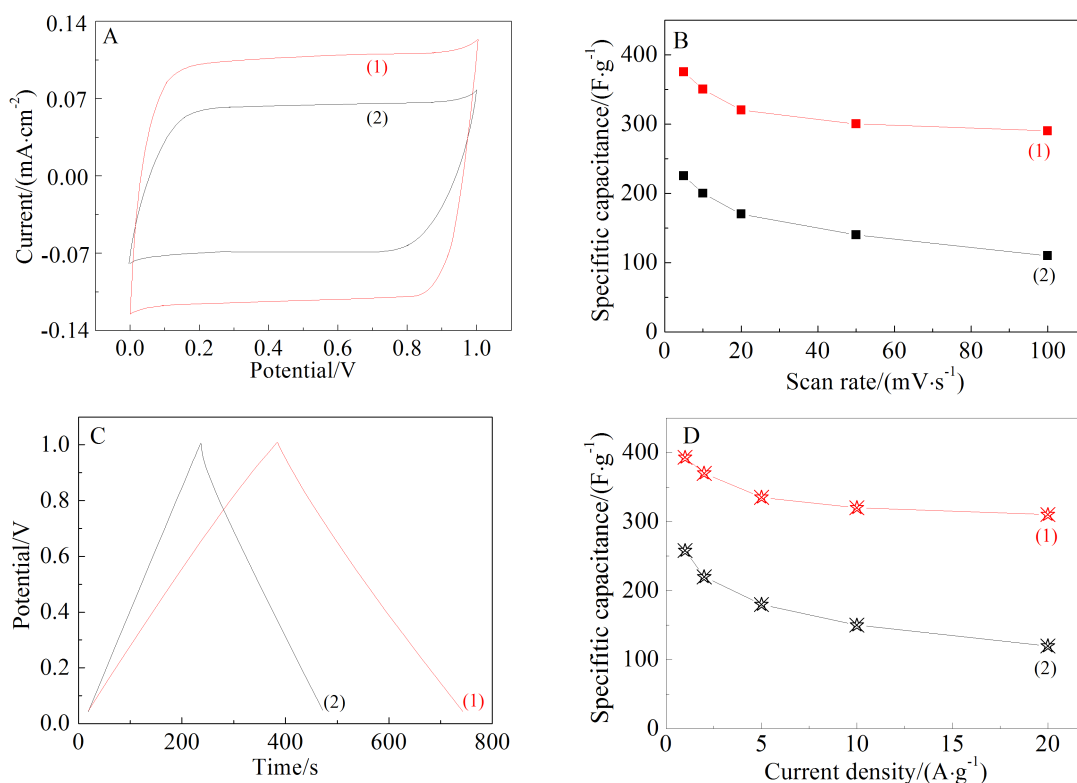


Fig. 4 A. CVs at 5 mV · s<sup>-1</sup>; B.  $C_{sp}$  as a function of scan rate; C. Galvanostatic charge-discharge curves at 1.0 A · g<sup>-1</sup>; D.  $C_{sp}$  as a function of current densities for the RGO hollow network cages (1) and the RGO films (2)



network cages at  $5 \text{ mV} \cdot \text{s}^{-1}$  is calculated to be  $374 \text{ F} \cdot \text{g}^{-1}$ , which is much higher than  $225 \text{ F} \cdot \text{g}^{-1}$  of RGO films. Even at a scan rate as high as  $100 \text{ mV} \cdot \text{s}^{-1}$ , the RGO hollow network cages could still achieve a  $C_{\text{sp}}$  as large as  $289 \text{ F} \cdot \text{g}^{-1}$ , which is also much larger than  $110 \text{ F} \cdot \text{g}^{-1}$  of RGO films. The dependence of  $C_{\text{sp}}$  on scan rate is shown in Fig. 4B, which shows a high rate capability of RGO hollow network cages and a small decay of only 28% in  $C_{\text{sp}}$  with scan rate increasing from 5 to  $100 \text{ mV} \cdot \text{s}^{-1}$ . Galvanostatic chargedischarge curves of the RGO hollow network cages were further measured as shown in Fig. 4C. A symmetric nature is observed in charging/discharging curves, indicating a superior electrochemical capacitive characteristic. The summary plot of  $C_{\text{sp}}$  vs current density is shown in Fig. 4D. When the current density was  $1.0 \text{ A} \cdot \text{g}^{-1}$ , the  $C_{\text{sp}}$  of RGO hollow network cages achieved  $393 \text{ F} \cdot \text{g}^{-1}$ , which is much larger than that of RGO films and those of other graphene materials, such as macroporous graphene frame works, mesoporous graphene nanofibers and graphene nanosheets<sup>[11,152743-45]</sup>. When the current density increased to  $20 \text{ A} \cdot \text{g}^{-1}$ , the  $C_{\text{sp}}$  of RGO hollow network cages still remained  $310 \text{ F} \cdot \text{g}^{-1}$ . With the charging-discharging rate increasing from  $1.0$  to  $20 \text{ A} \cdot \text{g}^{-1}$ , the RGO hollow network cages only showed 21.2% loss in  $C_{\text{sp}}$ , which is much smaller than 53.4% loss of RGO films and those of other graphene materials<sup>[11,152743-45]</sup>. Therefore, the RGO hollow network cages as electrodes exhibited large  $C_{\text{sp}}$  and excellent rate capability for SCs.

The above results demonstrate that the RGO hollow network cages allowed to maximize the performance of graphene. Here, it is believed that the ideal hollow network cage configurations have important contributions to high  $C_{\text{sp}}$  and excellent rate capability. This can be explained as following: firstly, the RGO hollow network cages with anisotropic morphology, large surface area, hollow structures and network cage structures can create efficient diffusion paths for electrolyte ions, which will significantly enhance the intercalation of electrolyte ions and the utilization rate of electrode material. Secondly, the conductive network in graphene material is well-built be-

cause of the network cage structures, and this will highly favor electron transmission during charging and discharging processes. The small diffusive resistance of electrolyte ions and small faradic charge transfer resistance in the RGO hollow network cages are well proved by the Nyquist plot shown in Fig. 5A. The intercept at the real axis of the plot corresponds to the solution resistance ( $R_s$ ) that is small and is only  $0.77 \Omega$ . The slope of a straight line in low frequency region can reflect the diffusive resistance resulting from the diffusion of active species in the electrolyte<sup>[46-47]</sup>. Here the RGO hollow network cages show almost vertical line in low frequency region as shown in Fig. 5A, indicating the small diffusive resistance of electroactive species in electrolyte. In addition, the conspicuous semicircle in the high-frequency range is not seen and only a line is observed, indicating the faradic charge transfer resistance ( $R_{\text{ct}}$ ) is very small<sup>[48]</sup>. Therefore, the above results indicate the perfect ion diffusion and charge transmission in the RGO hollow network cages, which are very helpful to large  $C_{\text{sp}}$  and excellent rate capability.

The excellent long-term cycle stability of RGO hollow network cages is demonstrated for SCs. The variation in  $C_{\text{sp}}$  of the RGO hollow network cages as a function of cycle number is shown in Fig. 5B, which shows the RGO hollow network cages could withstand over 10000 cycles with almost no decrease in  $C_{\text{sp}}$  ( $< 1\% C_{\text{sp}}$  loss). To further investigate the rate capability of RGO hollow network cages, we tested their cycling performances at progressively changed current densities, and the results are given in Fig. 5C. Even electrode material suffered from sudden current density change, the RGO hollow network cages still showed the stable  $C_{\text{sp}}$  at each current density. The above results further demonstrate that the synthesized RGO hollow network cages could meet the requirements of both long cycle lifetime and good rate capability, which are highly important for the applications in the practical energy storage devices.

To demonstrate their feasibility for energy storage applications, a simple solid-state flexible SC was assembled based on two pieces of RGO hollow net-

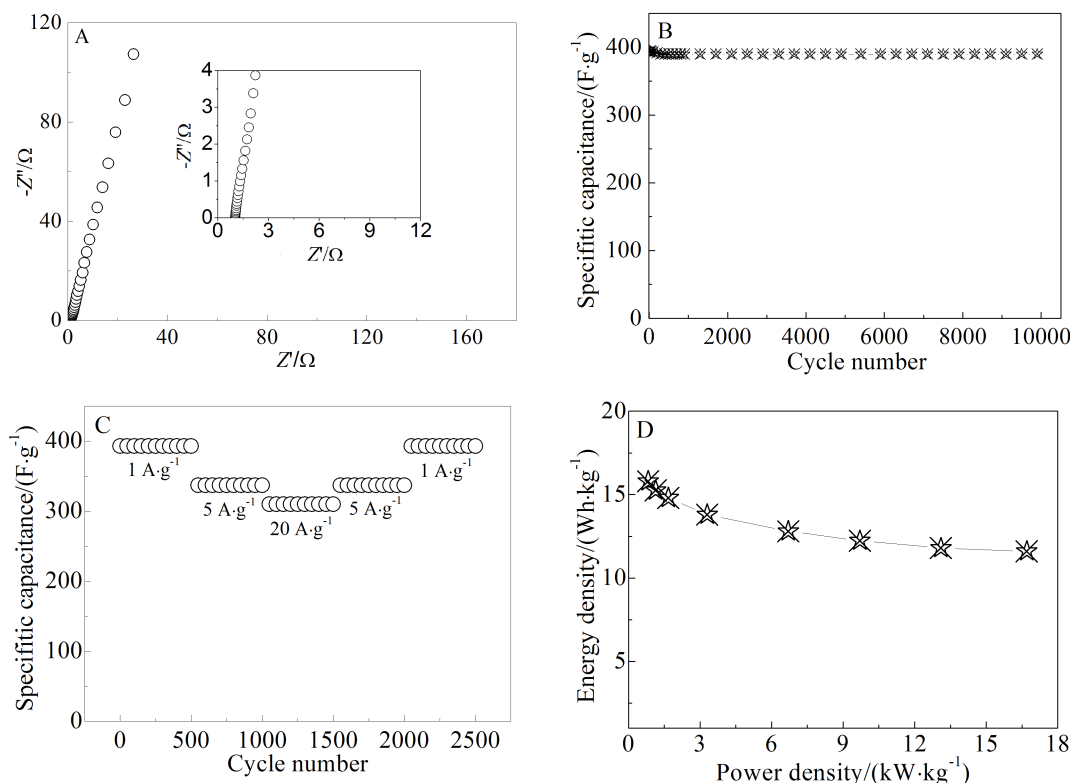


Fig. 5 A. EIS of RGO hollow network cages measured at open circuit potential in the frequency range from 0.01 to 105 Hz; B. Cycling performance of RGO hollow network cages during 10000 cycles at  $1.0 \text{ A} \cdot \text{g}^{-1}$ ; C. Cycling stability of RGO hollow network cages at progressively varied current densities; D. Ragone plot of a simple solid-state flexible SC that was assembled based on two pieces of RGO hollow network cage electrodes

work cage electrodes. The capacitive properties of the fabricated device were studied by cyclic voltammetry in a two-electrode system. As shown in Fig. S5, a typical double-layer capacitive behavior was observed. The  $C_{\text{sp}}$  value of the assembled SC was  $\sim 122 \text{ F} \cdot \text{g}^{-1}$  at a scan rate of  $5 \text{ mV} \cdot \text{s}^{-1}$ . Ragone plot is shown in Fig. 5D, which demonstrates the good rate performance of the assembled SCs with high energy and power densities. For instance, at a current density of  $20 \text{ A} \cdot \text{g}^{-1}$ , the energy density and power density of the assembled SC were  $12.4 \text{ Wh} \cdot \text{kg}^{-1}$  and  $9.7 \text{ kW} \cdot \text{kg}^{-1}$ , respectively. Significantly, the assembled SC showed a higher power density of  $16.7 \text{ kW} \cdot \text{kg}^{-1}$  (energy density of  $11.6 \text{ Wh} \cdot \text{kg}^{-1}$ ) at a current density of  $100 \text{ A} \cdot \text{g}^{-1}$ , which is much higher than those of other graphene-based SCs reported previously (e.g., graphene frameworks,  $5.0 \text{ kW} \cdot \text{kg}^{-1}$ ; graphene film pillared by carbon black nanoparticles,  $5.1 \text{ kW} \cdot \text{kg}^{-1}$ )<sup>[49-50]</sup>. In addition, the assembled SC exhibited superior long-term cycle stability as shown in Fig. S9, which only shows  $\sim 5\%$   $C_{\text{sp}}$

loss after 10000 cycles.

### 3 Conclusions

In summary, here we firstly demonstrated the synthesis of novel RGO hollow network cages by ZnO template assisted electrochemical reduction of GO. The synthesized hollow network cages could effectively prevent RGO from restacking and impart large surface area, high transport rate of electroactive species, high utilization rate of electrode, and high electrical conductivity. The electrochemical measurements confirmed the superior capacitive performance of the RGO hollow network cages, such as high  $C_{\text{sp}}$ , superior rate capability and excellent long-term cycle stability. Here the reported design concept of hollow network cages can be utilized for metal oxides or organic materials, such as  $\text{MnO}_2$  and polyaniline, to build the multifunctional hollow nanostructures, which will be promising for a large spectrum of device applications.

## Supporting Information Available

The Supporting Information is available free of charge via the Internet at <http://electrochem.xmu.edu.cn>.

## References:

- [1] Shi J L, Du W C, Yin Y X, et al. Hydrothermal reduction of three-dimensional graphene oxide for binder-free flexible supercapacitors[J]. *Journal of Materials Chemistry A*, 2014, 2(28): 10830-10834.
- [2] Bo Z, Zhu W G, Ma W, et al. Vertically oriented graphene bridging active-layer/current-collector interface for ultrahigh rate supercapacitors[J]. *Advanced Materials*, 2013, 25(40): 5799-5806.
- [3] Wang R T, Lang J W, Yan X B. Effect of surface area and heteroatom of porous carbon materials on electrochemical capacitance in aqueous and organic electrolytes[J]. *Science China Chemistry*, 2014, 57(11): 1570-1578.
- [4] Xin S, Guo Y G, Wan L J. Nanocarbon networks for advanced rechargeable lithium batteries[J]. *Accounts of Chemical Research*, 2012, 45(10): 1759-1769.
- [5] Wu Z S, Sun Y, Tan Y Z, et al. Three-dimensional graphene-based macro-and mesoporous frameworks for high-performance electrochemical capacitive energy storage[J]. *Journal of the American Chemical Society*, 2012, 134(48): 19532-19535.
- [6] Cheng Y W, Lu S T, Zhang H B, et al. Synergistic effects from graphene and carbon nanotubes enable flexible and robust electrodes for high-performance supercapacitors[J]. *Nano Letters*, 2012, 12(8): 4206-4211.
- [7] Xu Z, Zhang Y, Li P G, et al. Strong, conductive, lightweight, neat graphene aerogel fibers with aligned pores[J]. *ACS Nano*, 2012, 6(8): 7103-7113.
- [8] Choi B G, Yang M, Hong W H, et al. 3D macroporous graphene frameworks for supercapacitors with high energy and power densities[J]. *ACS Nano*, 2012, 6(5): 4020-4028.
- [9] Jung N, Kwon S, Lee D, et al. Synthesis of chemically bonded graphene/carbon nanotube composites and their application in large volumetric capacitance supercapacitors[J]. *Advanced Materials*, 2013, 25(47): 6854-6858.
- [10] Fan Z J, Yan J, Zhi L J, et al. A three-dimensional carbon nanotube/graphene sandwich and its application as electrode in supercapacitors[J]. *Advanced Materials*, 2010, 22(33): 3723-3728.
- [11] Liu F, Song S Y, Xue D F, et al. Folded structured graphene paper for high performance electrode materials [J]. *Advanced Materials*, 2012, 24(8): 1089-1094.
- [12] Zeng F Y, Kuang Y F, Wang Y, et al. Facile preparation of high-quality graphene scrolls from graphite oxide by a microexplosion method[J]. *Advanced Materials*, 2011, 23(42): 4929-4932.
- [13] Weng Z, Su Y, Wang D W, et al. Graphene-cellulose paper flexible supercapacitors[J]. *Advanced Energy Materials*, 2011, 1(5): 917-922.
- [14] Beidaghi M, Wang C. Micro-supercapacitors based on interdigital electrodes of reduced graphene oxide and carbon nanotube composites with ultrahigh power handling performance[J]. *Advanced Functional Materials*, 2012, 22(21): 4501-4510.
- [15] Lee J H, Park N, Kim B G, et al. Restacking-inhibited 3D reduced graphene oxide for high performance supercapacitor electrodes[J]. *ACS Nano*, 2013, 7(10): 9366-9374.
- [16] Lee J S, Kim S I, Yoon J C, et al. Chemical vapor deposition of mesoporous graphene nanoballs for supercapacitor[J]. *ACS Nano*, 2013, 7(7): 6047-6055.
- [17] Wen Z H, Wang X C, Mao S, et al. Crumpled nitrogen-doped graphene nanosheets with ultrahigh pore volume for high-performance supercapacitor[J]. *Advanced Materials*, 2012, 24(41): 5610-5616.
- [18] Wu Z S, Winter A, Chen L, et al. Three-dimensional nitrogen and boron co-doped graphene for high-performance all-solid-state supercapacitors[J]. *Advanced Materials*, 2012, 24(37): 5130-5135.
- [19] Yu D S, Dai L M. Self-assembled graphene/carbon nanotube hybrid films for supercapacitors[J]. *Journal of Physical Chemistry Letters*, 2010, 1(2): 467-470.
- [20] Kotal M, Bhowmick A K. Multifunctional hybrid materials based on carbon nanotube chemically bonded to reduced graphene oxide[J]. *The Journal of Physical Chemistry C*, 2013, 117(48): 25865-25875.
- [21] Feng Y Y, Qin M M, Guo H Q, et al. Infrared-actuated recovery of polyurethane filled by reduced graphene oxide/carbon nanotube hybrids with high energy density[J]. *ACS Applied Materials & Interfaces*, 2013, 5(21): 10882-10888.
- [22] Xu Y X, Huang X Q, Lin Z Y, et al. One-step strategy to graphene/Ni(OH)<sub>2</sub> composite hydrogels as advanced three-dimensional supercapacitor electrode materials[J]. *Nano Res*, 2013, 6(1): 65-76.
- [23] Zhang L L, Zhao X, Stoller M D, et al. Highly conductive and porous activated reduced graphene oxide films for high-power supercapacitors[J]. *Nano Letters*, 2012, 12(4): 1806-1812.
- [24] Zhang L, Shi G Q. Preparation of highly conductive graphene hydrogels for fabricating supercapacitors with high rate capability[J]. *Journal of Physical Chemistry C*, 2011, 115(34): 17206-17212.



- [25] Chen J, Sheng K X, Luo P H, et al. Graphene hydrogels deposited in nickel foams for high-rate electrochemical capacitors[J]. *Advanced Materials*, 2012, 24(33): 4569-4573.
- [26] Niu Z Q, Zhang L, Liu L L, et al. All-solid-state flexible ultrathin micro-supercapacitors based on graphene [J]. *Advanced Materials*, 2013, 25(29): 4035-4042.
- [27] Yoon Y, Lee K, Baik C, et al. Anti-solvent derived non-stacked reduced graphene oxide for high performance supercapacitors[J]. *Advanced Materials*, 2013, 25(32): 4437-4444.
- [28] Zhao Y, Hu C G, Hu Y, et al. A versatile, ultralight, nitrogen-doped graphene framework[J]. *Angewandte Chemie International Edition*, 2012, 124(45): 11533-11537.
- [29] Chang H X, Wu H K. Graphene-based nanocomposites: Preparation, functionalization, and energy and environmental applications[J]. *Energy & Environmental Science*, 2013, 6(12): 3483-3507.
- [30] Moon G D, Joo J B, Yin Y D. Stacked multilayers of alternating reduced graphene oxide and carbon nanotubes for planar supercapacitors[J]. *Nanoscale*, 2013, 5(23): 11577-11581.
- [31] Tan Y B, Lee J M. Graphene for supercapacitor applications[J]. *Journal of Materials Chemistry A*, 2013, 1(47): 14814-14843.
- [32] Xu C H, Xu B H, Gu Y, et al. Graphene-based electrodes for electrochemical energy storage[J]. *Energy & Environmental Science*, 2013, 6(5): 1388-1414.
- [33] Zhang J, Zhao F, Zhang Z P, et al. Dimension-tailored functional graphene structures for energy conversion and storage[J]. *Nanoscale*, 2013, 5(8): 3112-3126.
- [34] Li Y R, Sheng K X, Yuan W J, et al. A high-performance flexible fibre-shaped electrochemical capacitor based on electrochemically reduced graphene oxide[J]. *Chemical Communications*, 2013, 49(3): 291-293.
- [35] Zhang L L, Zhao X, Ji H X, et al. Nitrogen doping of graphene and its effect on quantum capacitance, and a new insight on the enhanced capacitance of N-doped carbon[J]. *Energy & Environmental Science*, 2012, 5(11): 9618-9625.
- [36] Choi B G, Chang S J, Kang H W, et al. High performance of a solid-state flexible asymmetric supercapacitor based on graphene films[J]. *Nanoscale*, 2012, 4(16): 4983-4988.
- [37] Chen C M, Zhang Q, Zhao X C, et al. Hierarchically aminated graphene honeycombs for electrochemical capacitive energy storage[J]. *Journal of Materials Chemistry*, 2012, 22(28): 14076-14084.
- [38] Zeng F Y, Kuang Y F, Liu G Q, et al. Supercapacitors based on high-quality graphene scrolls[J]. *Nanoscale*, 2012, 4(13): 3997-4001.
- [39] Guo H L, Wang X F, Qian Q Y, et al. A green approach to the synthesis of graphene nanosheets[J]. *ACS Nano*, 2009, 3(9): 2653-2659.
- [40] Haque A M, Park H, Sung D, et al. An electrochemically reduced graphene oxide-based electrochemical immunosensing platform for ultrasensitive antigen detection[J]. *Analytical Chemistry*, 2012, 84(4): 1871-1878.
- [41] Sheng K X, Sun Y Q, Li C, et al. Ultrahigh-rate supercapacitors based on electrochemically reduced graphene oxide for ac line-filtering[J]. *Scientific Reports*, 2012, 2: 247.
- [42] Xue Y Z, Wu B, Jiang L, et al. Low temperature growth of highly nitrogen-doped single crystal graphene arrays by chemical vapor deposition[J]. *Journal of the American Chemical Society*, 2012, 134(27): 11060-11063.
- [43] Cui C J, Qian W Z, Yu Y T, et al. Highly electroconductive mesoporous graphene nanofibers and their capacitance performance at 4 V[J]. *Journal of the American Chemical Society*, 2014, 136(6): 2256-2259.
- [44] Parvez K, Wu Z S, Li R J, et al. Exfoliation of graphite into graphene in aqueous solutions of inorganic salts[J]. *Journal of the American Chemical Society*, 2014, 136(16): 6083-6091.
- [45] Wang C L, Zhou Y, Sun L, et al. N/P-codoped thermally reduced graphene for high-performance supercapacitor applications[J]. *The Journal of Physical Chemistry C*, 2013, 117(29): 14912-14919.
- [46] Lang J W, Yan X B, Liu W W, et al. Influence of nitric acid modification of ordered mesoporous carbon materials on their capacitive performances in different aqueous electrolytes[J]. *Journal of Power Sources*, 2012, 204: 220-229.
- [47] Li M, Xu S H, Liu T, et al. Electrochemically-deposited nanostructured  $\text{Co}(\text{OH})_2$  flakes on three-dimensional ordered nickel/silicon microchannel plates for miniature supercapacitors[J]. *Journal of Materials Chemistry A*, 2013, 1(3): 532-540.
- [48] Justin P, Meher S K, Rao G R. Tuning of capacitance behavior of NiO using anionic, cationic, and nonionic surfactants by hydrothermal synthesis[J]. *The Journal of Physical Chemistry C*, 2010, 114(11): 5203-5210.
- [49] Xiao N, Tan H T, Zhu J X, et al. High-performance supercapacitor electrodes based on graphene achieved by thermal treatment with the aid of nitric acid[J]. *ACS Applied Materials & Interfaces*, 2013, 5(8): 9656-9662.
- [50] Wang G K, Sun X, Lu F Y, et al. Flexible pillared graphene-paper electrodes for high-performance electrochemical supercapacitors[J]. *Small*, 2011, 8(3): 452-459.

# 具有高效电化学储能的中空网状笼还原氧化石墨烯

张 翹,何序骏,李高仁\*

(中山大学化学与化学工程学院,广东 广州 510275)

**摘要:**通过 ZnO 模板辅助电沉积法制备了中空网状笼还原氧化石墨烯,具有纳米管、多孔结构、网状结构和 3D 微米中空笼等多层次架构. 这样的结构能够同时促进电化学活性物种的传输,提高电极材料的利用率,以及提升超级电容器性能. 该类中空网状笼还原氧化石墨烯做超级充电器电极材料时表现出了优良的电化学性能,研究结果显示,在  $1.0 \text{ A} \cdot \text{g}^{-1}$  时比电容达到  $393 \text{ F} \cdot \text{g}^{-1}$ . 而且当电流密度从  $1.0 \text{ A} \cdot \text{g}^{-1}$  增加到  $20 \text{ A} \cdot \text{g}^{-1}$ ,电容仅衰减了 21.2%,10000 周循环后比电容损失小于 1%,表明具有优异的电容稳定性.

**关键词:**还原氧化石墨烯;多孔结构;纳米片;超级电容器